

Article

SMAD1 Is Dispensable for CDX2 Induction but Required for the Repression of Ectopic Small-Intestinal Gene Expression in Human-Pluripotent-Stem-Cell-Derived Colonic Organoids

Na Qu [†], Abdelkader Daoud [†], Braxton Jeffcoat and Jorge O. Múnera ^{*}

Department of Regenerative Medicine and Cell Biology, Medical University of South Carolina, Charleston, SC 29425, USA; qu@musc.edu (N.Q.); abdelkader.daoud@sickkids.ca (A.D.)

^{*} Correspondence: munera@musc.edu[†] These authors contributed equally to this work.

Abstract: The generation of gastrointestinal tissues from human pluripotent stem cells has provided unprecedented insight into the molecular mechanisms that drive the patterning of the primitive gut tube. Previous work has identified bone-morphogenetic-protein (BMP) signaling as an important mediator of mid/hindgut versus foregut and hindgut versus midgut cell fate choice. Inhibition of BMP signaling during gut tube morphogenesis inhibits the expression of the pan-intestinal transcription factor CDX2. Treatment of CDX2+ mid/hindgut cultures with BMP patterns them into hindgut, which gives rise to colonic organoids (HCOs). While the role for BMP signaling is clear, the molecular mechanisms through which BMP signaling patterns the mid/hindgut and colon remain unclear. BMPs bind to BMP receptors, activating a signaling cascade that results in the activation of SMADs, which function as transcription factors. We hypothesized that one of these factors, SMAD1, would be necessary for establishing the CDX2 domain and the colon domain. Unexpectedly, endoderm derived from SMAD1-deficient induced pluripotent stem cells was capable of inducing CDX2 in response to WNT and FGF signaling. In addition, CDX2+ gut tube cultures could activate posterior HOX genes in response to BMP. However, examination of HCOs following cytodifferentiation revealed that SMAD1-deficient HCOs ectopically expressed small-intestinal markers despite expressing posterior HOX genes. These results indicate that there is redundancy of SMADs during early hindgut patterning but that SMAD1 is required for the inhibition of small-intestinal gene expression in HCOs.

Keywords: human pluripotent stem cells; colonic organoids; definitive endoderm; hindgut



Citation: Qu, N.; Daoud, A.; Jeffcoat, B.; Múnera, J.O. SMAD1 Is Dispensable for CDX2 Induction but Required for the Repression of Ectopic Small-Intestinal Gene Expression in Human-Pluripotent-Stem-Cell-Derived Colonic Organoids. *Organoids* **2023**, *2*, 192–203. <https://doi.org/10.3390/organoids2040015>

Academic Editor: Toshio Takahashi

Received: 3 September 2023

Revised: 26 October 2023

Accepted: 7 November 2023

Published: 14 November 2023



Copyright: © 2023 by the authors. Licensee MDPI, Basel, Switzerland. This article is an open access article distributed under the terms and conditions of the Creative Commons Attribution (CC BY) license (<https://creativecommons.org/licenses/by/4.0/>).

1. Introduction

Over the past 4 decades, advances in stem cell biology have resulted in the generation of multiple protocols for the differentiation of human pluripotent stem cells (hPSCs) into various tissues. In terms of endoderm-derived organs, protocols are now in place that allow the generation of nearly all organs within the gastrointestinal tract. This includes organoids that resemble the esophagus [1], gastric fundus [2], gastric antrum [3], proximal small intestine [4], distal small intestine [5], and colon [6,7]. Generation of these organoids requires differentiation of hPSCs first into definitive endoderm, then into the correct region of the gut tube, and then optimizing the growth conditions for the given organ. These differentiations require the temporal addition of specific growth factors that mimic normal organ development.

The bone-morphogenetic-protein (BMP) pathway is critical for the development of the intestine and colon as well as maintenance of homeostasis in adult tissue [8,9]. In addition, BMP signaling regulates multiple processes during intestinal development, including establishment of proliferative progenitor domains [10,11], villus emergence [10,11], and establishment of the crypt–villus axis in the intestine and colon. BMPs signal through heteromeric complexes formed by type I and type II BMP receptors. Upon ligand binding,

activated BMP type I receptors phosphorylate receptor SMADs (R-SMADs) 1/5/9, which then bind the co-SMAD, SMAD4. Upon binding to SMAD4, the R-SMAD/SMAD4 complex is then translocated to the nucleus, where it can activate or repress gene transcription by recruiting RNA POLII complexes and by modulating local chromatin structure through interaction with chromatin modifiers and co-activators. Several studies in model organisms have implicated the BMP signaling pathway in patterning endoderm during hindgut development [12,13]. Furthermore, inhibition of BMP signaling during the generation of mid/hindgut generated from hPSCs results in the generation of three-dimensional foregut spheroids, which can be further differentiated into gastric [2,3] or lung tissue [14].

Despite the clear roles of BMP signaling in intestinal development, how SMADs regulate these developmental processes has not been fully elucidated. Based on mouse studies, SMAD1 and SMAD5 are the most critical SMADs for proper murine development. Therefore, we hypothesized that SMAD1 deficiency would result in the loss of generation of mid/hindgut tissue from pluripotent stem cells. We generated SMAD1-deficient iPSCs, and we found that the induction of CDX2 by WNT and FGF was not disturbed by SMAD1 deficiency. In addition, we found that early patterning of CDX2+ cultures into posterior hindgut tissue was not altered by SMAD1 deficiency. However, extended growth of WT and SMAD1-deficient HCOs revealed that SMAD1 deficiency resulted in altered mesoderm differentiation and ectopic expression of small-intestinal genes. These results indicate that SMAD1 is dispensable for early hindgut patterning, possibly due to redundancy with other SMADs.

2. Materials and Methods

2.1. Cell Culture

The human induced pluripotent stem cell lines K3 WT and K3 SMAD1^{-/-} were obtained from Medical University of South Carolina Cell Models Core. iPSCs were grown in feeder-free conditions in six-well Nunclon[®] surface plates (Nunc) coated with Matrigel (BD Biosciences, Franklin Lakes, NJ, USA) and maintained in mTeSR1 media (Stem Cell Technologies, Vancouver, BC, Canada) at 37 °C with 5% CO₂. The K3 line has been previously characterized [15]. Cells were passaged every 4 days using a dispase solution (Thermo Fisher Scientific, Waltham, MA, USA) and were checked daily for differentiation. The cell line was checked for karyotype and routinely checked for mycoplasma.

2.2. Generation of SMAD1-Deficient Cells

Guide RNA sequences were cloned into the PX459 pSPCas9(BB)-2A-Puro vector (pSpCas9(BB)-2A-Puro (PX459) V2.0 was a gift from Feng Zhang (Addgene plasmid # 62988; RRID:Addgene_62988)). The CRISPR-Cas9/gRNA plasmid and the homology oligo containing a stop codon were transfected into K3 induced pluripotent cells using Lipofectamine 3000 (Thermo Fisher Scientific, Los Angeles, CA, USA), following the manufacturer's protocol. After 24 h, cells were selected on 1 µg/mL of puromycin (Sigma Aldrich, St. Louis, MO, USA) for 48 h. Cells were then expanded, passaged, and plated at clonal density. Clones were selected and then expanded. K3 cells were then grown in Nunclon[®] surface plates (Nunc) coated with Matrigel (BD Biosciences), as detailed above. Colony 18 was grown, and cells were collected. Genomic DNA from cells was extracted using a QIAamp DNA Mini Kit (Qiagen, Hilden, Germany), following the manufacturer's protocol. Purified genomic DNA was sent to GENEWIZ for sequencing based on the gRNA and oligo information we provided.

2.3. Generation of Human Gut Tube Cultures

Human mid/hindgut cultures were generated as previously described [4,16,17]. For definitive endoderm (DE) induction, iPSCs were passaged with Accutase (Invitrogen, Waltham, MA, USA) and plated at a density of 100,000 cells per well in a Matrigel-coated, Nunclon[®] surface, 24-well plate. On the first day of splitting, 10 µM of Y27632 compound (Sigma) was added to the mTeSR1 media. After 24 h, media was changed to mTeSR1, and

cells were grown for an additional 24 h. Then, the cells were treated with 100 ng/mL of Activin A for 3 days as previously described for DE formation, except that BMP4 (R&D) was added to day 1 at a concentration of 15 ng/mL [4]. DE was then treated with hindgut induction medium (RPMI 1640, 2 mM L-glutamine, 2% decomplemented FBS) for 4 d with 500 ng/mL of FGF4 (R&D) and 3 μ M of Chiron 99021 (Tocris, Bristol, UK) to induce the formation of mid/hindgut endoderm, which remained in a monolayer.

2.4. Three-Dimensional Culture and Posterior Patterning of Dissociated Mid/Hindgut Endoderm

Clumps were generated from the mid/hindgut endoderm monolayer as detailed previously [18]. Briefly, the monolayer was scraped from the 24-well tissue culture plate using 1000 μ L pipet tips. The resulting clumps were then transferred to 15 mL tubes and further triturated by continuous pipetting using a 1000 μ L pipet. The resulting clumps were then filtered through a 200 μ m cell strainer (Pluriselect, Leipzig, Germany). Clumps that passed through the 200 μ m cell strainer into the flowthrough were plated in Matrigel in a 24-well plate. To generate proximal HIOs, spheroids or clumps were overlaid with intestinal growth medium (Advanced DMEM/F-12, N2, B27, 15 mM HEPES, 2 mM L-glutamine, penicillin-streptomycin) supplemented with 100 ng/mL of EGF (R&D) alone or 100 ng/mL of EGF + 100 ng/mL of BMP2 for 3 days. For the BMP2 + LDN organoids, LDN193189 was added at a concentration of 300 nM. After the 3 days of patterning, media was replaced every 2–3 days with intestinal growth medium with 100 ng/mL of EGF. Organoids were split on day 21 and were cultured with media replacement every 2–3 days up the 35-day timepoint.

For 2 and 6 h patterning experiments, following generation of mid/hindgut endoderm, organoids were plated in Matrigel and then treated with the same concentration of BMP2 as detailed above. DMH-1 was used at a concentration of 20 μ M. Cycloheximide (CHX) was used at a concentration of 50 μ g/mL. LDN193189 was used at a concentration of 300 nM. The Nucleospin[®] RNA extraction kit (Macharey-Nagel, Düren, Germany) and cDNA using Superscript VILO (Invitrogen) were both used according to the manufacturers' protocols. Primer sequences are listed in Supplementary Table S1. QPCR was performed using the Quantitect SYBR[®] Green PCR kit (Qiagen) and a CFX96 Touch Real-Time PCR Detection System (Biorad, Hercules, CA, USA). For mid/hindgut clumps or 35-day-old organoids, 2–3 wells were collected per replicate. For genotyping of 35-day-old organoids, 4% PFA fixed organoids were washed with 1X PBS and then heated at 95 °C for 15 min in 180 μ L of 50 mM NaOH. Samples were then cooled, and 20 μ L of 1 M Tris-HCL was added. Samples were then centrifuged, and 5 μ L was used as a template for PCR, which was performed with Phusion[®] High-Fidelity DNA Polymerase. The primer sequences for genotyping are provided in Supplementary Table S1. The PCR product was purified using a GeneJET Gel Extraction Kit (Thermo Scientific) and then digested with EcoRI (New England Biolabs, Ipswich, MA, USA). Digested PCR products were run on an agarose gel containing SYBR Safe DNA dye (Thermo Scientific).

2.5. Immunofluorescence Staining

Organoids were fixed in 4% PFA, washed in PBS, and then placed in 30% sucrose overnight at 4 °C on a rocking platform. Organoids were then frozen in OCT. After cryosection, the slides with tissues were blocked using normal donkey serum (5% serum in 1X PBS plus 0.5% Triton-X) for 30 min at room temperature. Then, the tissues were incubated with primary antibody overnight at 4 °C. The next day, slides were washed 3X with 1X PBS plus 0.5% Triton-X (PBST) and incubated in secondary antibody with DAPI in blocking buffer for 2 h at room temperature. Please see Supplementary Table S2 for a list of antibodies and respective dilutions. Slides were then washed 2X with PBST, followed by a final wash in 1X PBS. Coverslips were then mounted using Fluoromount-G[®] (SouthernBiotech, Birmingham, AL, USA). Images were captured on a Zeiss LSM 880 NLO with Airscan confocal microscope and analyzed using Imaris Bitplane Imaging Software Version 10 (Oxford Instruments, Oxfordshire, UK).

2.6. Western Blot

IPSCs grown in 6-well dishes were rinsed with ice-cold phosphate-buffered saline (PBS) and lysed with Triton buffer (40 mM HEPES pH 7.4, 150 mM NaCl, 2.5 mM MgCl₂, and 1% Triton) supplemented with protease inhibitor (Thermo Fisher Scientific, A32953) and phosphatase inhibitors (phosphatase inhibitor cocktail sets I and II, Calbiochem). The cell lysates were centrifuged at 13,200 r.p.m. for 10 min at 4 °C. Equal amounts of protein were separated by SDS-PAGE, transferred to a polyvinylidene difluoride membrane (Millipore), immunoblotted with antibodies, and visualized with horseradish-peroxidase-coupled secondary antibodies.

2.7. RNA-Seq Processing and Analysis

RNA was purified using the Nucleospin[®] RNA extraction kit (Macharey-Nagel) and sent to BGI for RNA library construction and RNA sequencing using the DNBseq platform. For sequencing data analysis, the 6 h control and BMP2 data were analyzed by BGI. The sequencing reads were filtered using the BGI internal software SOAPnuke to get clean reads, which were stored in FASTQ format. The clean reads were mapped to the human genome with HISAT2 and Bowtie2. Gene expression level was calculated with RSEM. DEseq2 was used to obtain differentially expressed gene data.

For clump derived 35-day-old organoids from, the Partek Flow software version 11 (Partek Inc., Chesterfield, MO, USA) was used for data analysis. Analysis was initiated from FASTQ files, and clean reads were mapped to the human genome with STAR and quantified to an annotation model using Partek E/M. DEseq2 was used to identify differentially expressed gene data. PCA was conducted in Partek Flow for the RNA-seq data sets. Morpheus (<https://software.broadinstitute.org/morpheus/>, accessed on 3 September 2023) was used to generate heatmaps from TPM values. ToppFun analysis was performed using (<https://toppgene.cchmc.org/enrichment.jsp>, accessed on 3 September 2023). Differentially expressed data identified by DEseq2 were used for ToppFun analysis.

3. Results

3.1. SMAD1-Deficient Induced Pluripotent Stem Cells Are Competent to Generate CDX2-Expressing Mid/Hindgut

To understand how BMP signaling regulates colonic patterning, we established SMAD1^{-/-} human IPSCs using CRISPR-Cas9-mediated gene targeting [19]. We introduced a stop codon into SMAD1 exon 2 using CRISPR-Cas9-mediated homology-directed repair (HDR) in IPSCs by introducing a guide RNA targeting exon 2, along with an oligo with homology to exon 2, except it included an EcoRI site and a stop codon (Figure 1A). Analysis of genomic DNA revealed the presence of mutations in SMAD1 in the SMAD1^{-/-} IPSCs (Figure 1B) when compared with WT. The WT sequence in SMAD1^{-/-} IPSCs was not detectable above background. We further verified that these cells lack the SMAD1 protein using a western blot (Figure 1C). We did not observe any differences in the growth of these cells. These results confirmed that our CRISPR-Cas9-mediated HDR strategy resulted in the generation of SMAD1^{-/-} IPSCs.

Previous studies reported that inhibition of BMP signaling (using the inhibitor NOGGIN) during the mid/hindgut induction step of the HIO protocol resulted in generation of CDX2-/SOX2+ foregut spheroids [2,3]. To determine whether SMAD1 is required for specification of CDX2+ mid/hindgut, we differentiated WT and SMAD1^{-/-} IPSCs into mid/hindgut using a standard protocol (Figure 2A). On day 7 of differentiation, we performed immunofluorescence staining of mid/hindgut monolayers using two different CDX2 antibodies and two different SOX2 antibodies. Surprisingly, both WT and SMAD1^{-/-} IPSCs were able to generate a CDX2+ monolayer that lacked SOX2 expression (Figure 2B,C). Our results indicate that SMAD1^{-/-} IPSCs are competent to generate CDX2+/SOX2- mid/hindgut tissue and suggest that in the absence of SMAD1, other SMADs may compensate for SMAD1 during mid/hindgut differentiation.

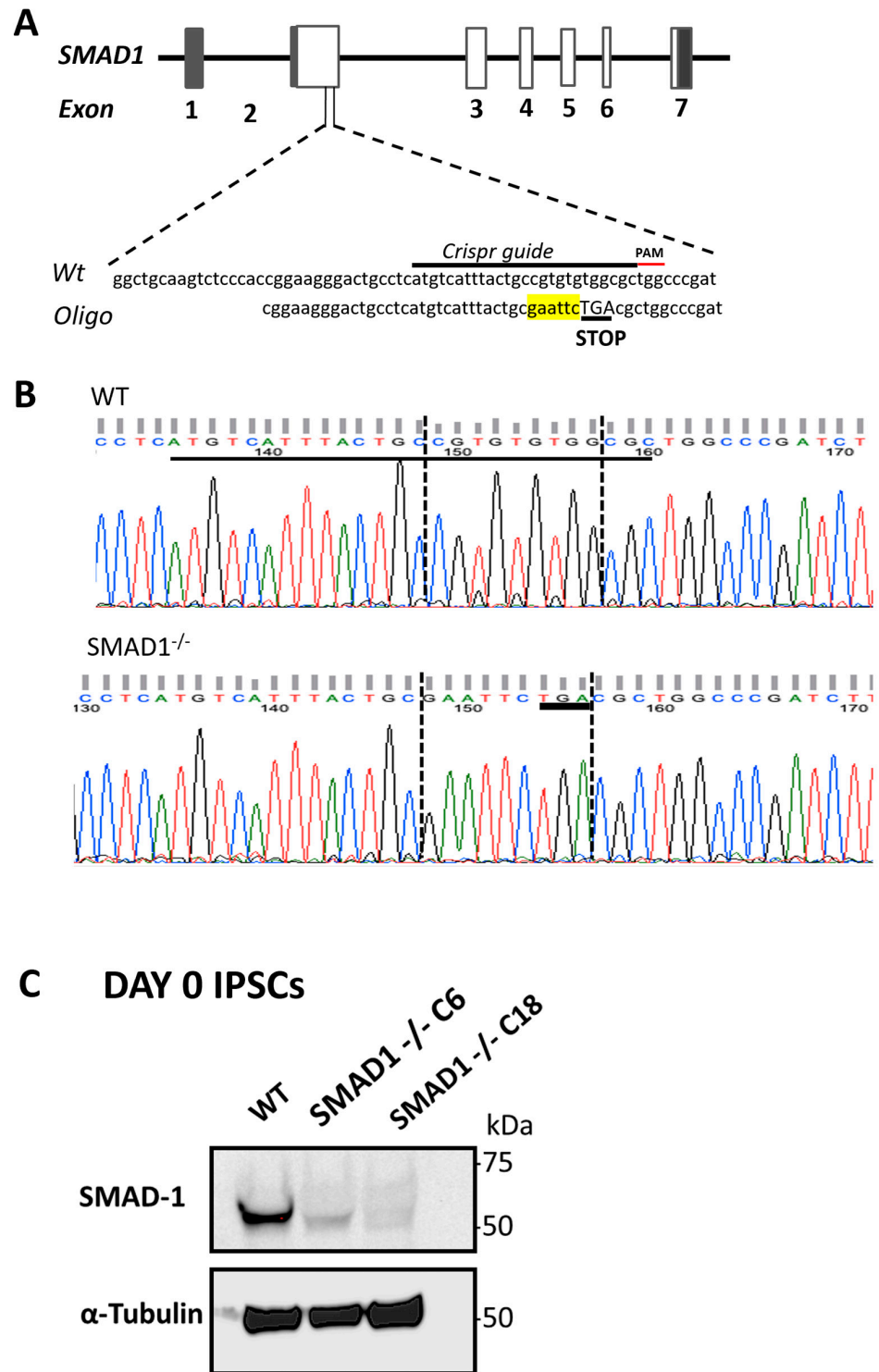


Figure 1. Generation and validation of SMAD1-deficient IPSCs. (A) Schematic describing the approach used to generate SMAD1^{-/-} IPSCs. CRISPR-Cas9 and HDR were used to insert a TGA stop codon into both alleles of SMAD1 exon 2. The sequences for the guide RNA and the oligo containing the homologous sequence to SMAD1 with an added stop codon (TGA) and an EcoRI cut site (highlighted in yellow). (B) DNA sequencing result comparing genomic DNA extracted from WT IPSCs and SMAD1-deficient IPSCs. (C) Western-blot analysis for SMAD1 protein in WT cells and 2 different colonies of SMAD1^{-/-} IPSCs. Sequencing results (B) were obtained from the C18 clone. All differentiations hereafter were performed with the C18 clone.

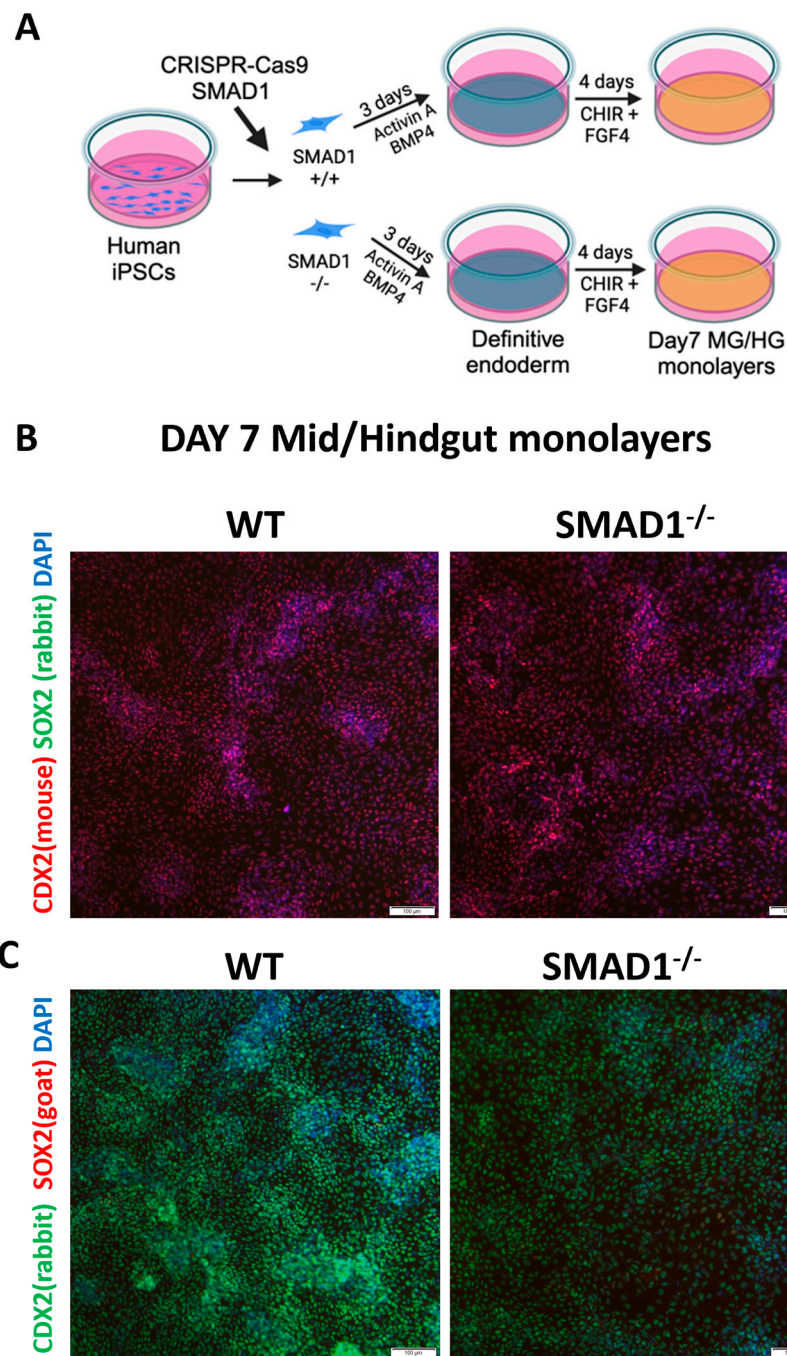


Figure 2. SMAD1-deficient iPSCs are competent to generate mid/hindgut tissue. **(A)** Schematic of mid/hindgut differentiation from WT and SMAD1 $^{-/-}$ iPSCs. **(B)** Immunostaining of day 7 mid/hindgut monolayers for CDX2 (red) and SOX2 (green), counterstained with DAPI (blue). Results are representative of 3 separate wells per condition. **(C)** Immunostaining of day 7 mid/hindgut monolayers for CDX2 (green) and SOX2 (red), counterstained with DAPI (blue). Results are representative of 3 separate wells per condition. Scale bars in B and C denote 100 microns.

3.2. Immediate Early and Late Targets of BMP Signaling Are Not Affected by SMAD1 Deficiency

To identify early transcriptional targets of BMP signaling, we treated mid/hindgut cultures $+/-$ BMP2 for 6 h and collected RNA for bulk RNA-seq (Figure 3A). We identified 12 genes that were differentially expressed in response to BMP2 (Figure 3B). To determine which of these genes were direct targets of BMP signaling, we treated mid/hindgut cultures for 2 h \pm BMP2, \pm DMH1 (an inhibitor of BMP type I receptors), and \pm cycloheximide (which

inhibits protein translation), and we performed qPCR on our newly identified target mRNAs (Figure 3C). We reasoned that (1) mRNAs, which are directly dependent on BMP signaling, would change after 2 h of BMP2 treatment, which is enough time for SMADs to activate gene expression [20]; (2) the BMP type I receptor inhibitor DMH1 should block the impact of BMP2 on any direct targets; and (3) if the observed change in expression of mRNAs is mediated directly by the action of SMADs, this will occur independently of protein synthesis, which can be inhibited by cycloheximide (CHX). Since CHX can impact the stability of mRNAs, +/- CHX samples were only compared with each other. Of the 12 mRNAs from our RNAseq analysis, we identified 7 whose expression was induced by BMP2 independently of protein synthesis (Figure 3D), indicating that they are direct targets of BMP signaling.

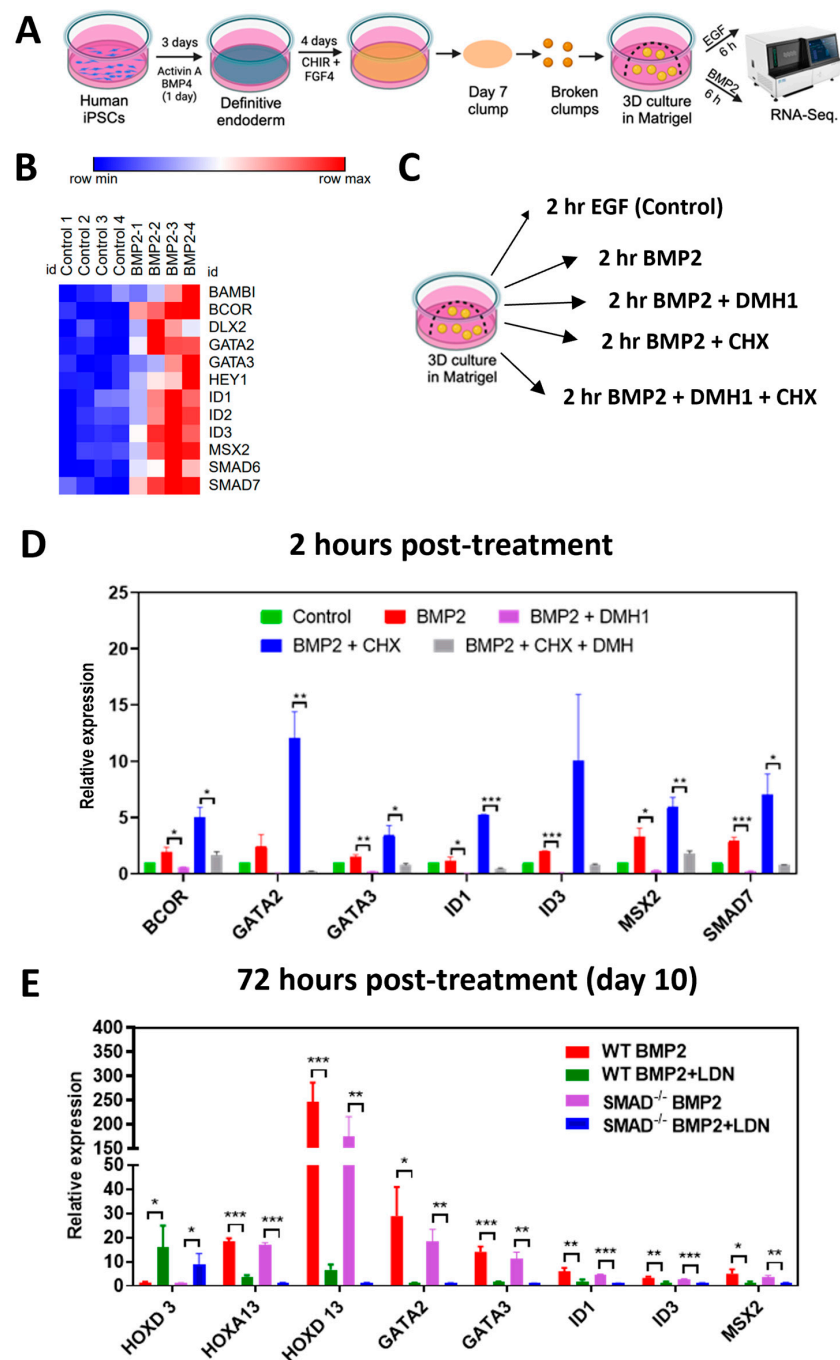


Figure 3. Posterior hindgut patterning is not altered in day 10 HCOs. (A) Schematic of mid/hindgut differentiation from WT and SMAD1^{-/-} IPSCs, followed by plating in Matrigel and 6 h of patterning.

Samples were collected for RNA sequencing. (B) Heatmap based on TPM (transcripts per million) values of mRNAs induced after 6 h of BMP2 treatment (BMP2 + EGF) or control (EGF only). (C) Schematic of experiment to identify direct targets induced by BMP2. DMH1 was used to inhibit signaling through BMP type I receptors. Cycloheximide (CHX) was used to block protein synthesis. (D) Quantitative PCR analysis of day 7 mid/hindgut spheroids that were plated in Matrigel and then treated with DMH1, media alone, BMP2, BMP2 + DMH1, BMP2 + CHX, or BMP2 + CHX + DMH1 for 2 h. N = 3. (E) Quantitative PCR analysis of day 7 mid/hindgut clumps from WT and SMAD1^{-/-} iPSCs plated in Matrigel. Cells were treated with BMP2 or BMP2 + LDN193189 (LDN is a BMP type I receptor inhibitor) for 72 h. * denotes $p < 0.05$, ** denotes $p < 0.01$, and *** denotes $p < 0.001$ by *t*-test in panels (D,E).

We next determined whether SMAD1 is required for the expression of the direct BMP target genes that we identified. In addition, we examined the mRNA expression of *HOX* factors, which are either repressed (*HOXD3*) or induced (*HOXA13* and *HOXD13*) in response to BMP induction for 3 days (Figure 3E). As expected, BMP induction repressed *HOXD3* mRNA expression and induced the expression of *HOXA13*, *HOXD13*, *GATA2*, *GATA3*, *ID1*, *ID3*, and *MSX2* mRNAs. Repression and induction of these genes were dependent on BMP type I receptors, as inhibition with the BMP type I receptor inhibitor LDN193189 blocked these effects. Surprisingly, the modulation of mRNA levels of these genes in SMAD1^{-/-} iPSCs compared with WT controls was not significantly different. This suggests that early colonic patterning can occur independently of SMAD1, suggesting that other SMADs may compensate for SMAD1 at this stage of HCO differentiation.

3.3. SMAD1-Deficient HCOs Ectopically Express Small-Intestinal Markers Following Long-Term Culture

We previously reported that a 3-day treatment of mid/hindgut cultures with BMP2 was sufficient to confer stable regional identity in organoids cultured until day 35. To determine if SMAD1-deficient organoids maintained posterior identity, we performed RNA-seq on day 35 organoids derived from WT and SMAD1^{-/-} iPSCs. Principal component analysis revealed that regardless of genotype, 35-day-old HCOs clustered along principal components 1, 2, and 3 (PC1, PC2, PC3), while HCOs that were treated with BMP in the presence of the BMP type I receptor inhibitor LDN193189 cluster together (Figure 4A). PC1, PC2, and PC3 accounted for 51% of the cumulative variation among samples. PCR-based genotyping confirmed that HCOs derived from SMAD1^{-/-} iPSCs remained SMAD1-deficient (Supplementary Figure S1). These results indicate that SMAD1 deficiency does not lead to overt effects on organoid patterning along the anterior–posterior axis.

To confirm that SMAD1^{-/-}-iPSC-derived HCOs were indeed patterned correctly, we examined the expression of anterior and posterior *HOX* genes. In addition, we also examined the colonic markers *SATB2* and *SATB2-AS1*. This analysis revealed that the mRNAs of the anterior *HOX* genes *HOXA2*, *HOXA3*, *HOXA4*, *HOXB2*, *HOXB3*, and *HOXD3* were all expressed at lower levels in organoids treated with BMP2 compared with those treated with BMP2 plus LDN193189, regardless of genotype (Figure 4B). In contrast, the mRNAs for posterior *HOX* genes *HOXA13* and *HOXD13*, along with *SATB2* and *SATB2-AS1*, were expressed at higher levels in organoids treated with BMP2 compared with those treated with BMP2 plus LDN193189, regardless of genotype. We further confirmed that SMAD1^{-/-} organoids were properly patterned by examining the expression of *SATB2*. Consistent with proper colonic patterning, SMAD1^{-/-} HCOs were positive for *SATB2* protein expression via immunofluorescence staining (Figure 4C). Taken together, these results indicate that SMAD1 deficiency does not overtly change colonic patterning of iPSCs.

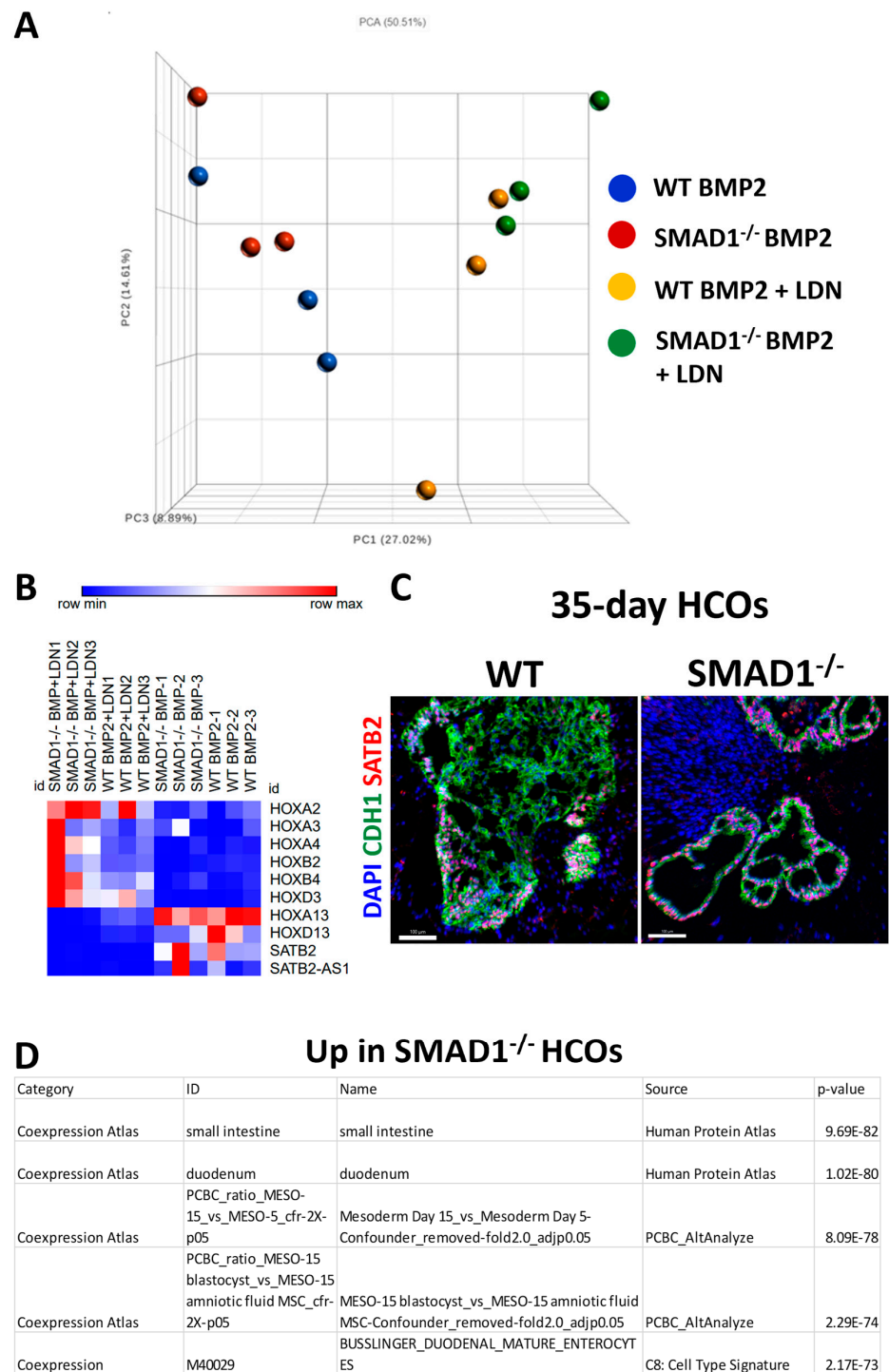


Figure 4. SMAD1-deficient HCOs retain posterior patterning but ectopically express small-intestinal markers. **(A)** Principal component analysis of 35-day-old organoids resulting from treatment of day 7 mid/hindgut clumps from WT and SMAD1^{-/-} iPSCs plated in Matrigel. Cells were treated with BMP2 or BMP2 + LDN193189 (LDN is a BMP type I receptor inhibitor) for 72 h. **(B)** Heatmap of anterior HOX genes, posterior HOX genes, SATB2, and SATB2-AS1 based on TPM (transcripts per million) values from RNA-seq data from the 35-day-old organoids that were analyzed in panel (A). **(C)** Immunofluorescence staining of 35-day-old HCOs derived from WT or SMAD1^{-/-} iPSCs. Sections were stained for CDH1 (green) and SATB2 (red) and were counterstained with DAPI. Images are representative of 5 organoids per genotype. Scale bars denote 100 microns. **(D)** Table of ToppFun results from gene list generated from DE-seq2 analysis comparing HCOs derived from WT or SMAD1^{-/-} iPSCs.

To determine the transcriptional differences between HCOs generated from WT and SMAD1^{-/-} iPSCs, we performed DE-seq2 analysis to generate a list of differentially expressed genes (Supplementary Table S3). We then performed tissue co-expression analysis (Supplementary Tables S4 and S5) using the ToppFun function in ToppGene (toppgene.cchmc.org, accessed on 3 September 2023). The top two co-expression IDs related to genes upregulated in SMAD1^{-/-} HCOs were small intestine and duodenum, which both exhibited a high level of significance (Figure 4D). We verified three of the up-regulated intestinal genes by qPCR and found that their mRNA levels were indeed increased in SMAD1^{-/-} HCOs (Supplementary Figure S2). In addition, co-expression atlas IDs related to mesoderm differentiation day 15 were related to genes upregulated in SMAD1^{-/-} HCOs compared with WT (Figure 4D). In summation, these results indicate that SMAD1 deficiency results in ectopic expression of proximal small-intestinal genes as well as altered differentiation of HCO mesenchyme.

4. Discussion

BMP signaling plays a known role in posterior–ventral patterning of endoderm [12,13,21–23]. However, few studies have extensively examined how SMADs mediate transcription downstream of BMP receptor activation by BMP ligands [24,25]. *Smad1*^{-/-} knockout mice die by embryonic day 10.5, which allows the analysis of early colonic patterning but precludes the analysis of intestinal and colonic cytodifferentiation. In this study, we tested the role of SMAD1 in mid/hindgut and colonic patterning by generating SMAD1-deficient iPSCs and differentiating them into human colonic organoids that resemble the e18.5 mouse colon. We found that SMAD1-deficient iPSCs could be differentiated into mid/hindgut endoderm and patterned into colonic organoids. However, HCOs derived from SMAD1-deficient iPSCs ectopically expressed small-intestinal mRNAs. This suggests that SMAD1 plays a role in repressing the expression of small-intestinal mRNAs in the colon.

BMP signaling can be transduced by SMAD1, SMAD5, and SMAD9. We chose to focus on *SMAD1* based on the requirement of *Smad1* for mouse embryonic development. Studies on mice suggest that SMAD1 and SMAD5 function cooperatively to activate gene expression downstream of BMP. *Smad1*^{+/-} and *Smad5*^{+/-} mice exhibit embryonic lethality at e10.5 [26]. This embryonic lethality is similar to the lethality observed in *Smad1*^{-/-} mice [27] and *Smad5*^{-/-} mice [28,29]. However, when *Smad9*^{-/-} knockout is combined with either *Smad1*^{+/-} or *Smad5*^{+/-}, mice are viable and fertile, similar to *Smad9*^{-/-} [26]. Furthermore, *Smad9*^{-/-} did not exacerbate the tissue disruptions observed *Smad1*^{-/-} mice or *Smad5*^{-/-} mice [26]. These data suggest that *Smad1* and *Smad5* are the most critical *Smads* during embryonic development. However, our results indicate that SMAD1 and SMAD5 have functional redundancy during mid/hindgut and colonic patterning. Redundancy of SMADs has been previously demonstrated in model systems [30,31].

Although our studies identified a role for SMAD1 in repression of small-intestinal mRNAs, we cannot pinpoint the developmental timepoint at which SMAD1 operates this function. There is also the possibility that SMAD1 deficiency results in organoids arresting in a developmental timepoint in which the fetal colon expresses small-intestinal brush border enzymes [32,33]. Future studies will require the conditional inactivation of *SMAD1* at different timepoints as well as examination of chromatin binding and accessibility to determine when and how SMAD1 functions to repress small-intestinal mRNAs. In addition, future studies will examine compound *SMAD1/SMAD5*-deficient cells to determine whether SMAD5 is redundant during early mid/hindgut patterning. In conclusion, our results indicate that SMAD1 is dispensable for early hindgut patterning and unveiled a role for SMAD1 in the inhibition of small-intestinal transcripts in HCOs.

Supplementary Materials: The following supporting information can be downloaded at <https://www.mdpi.com/article/10.3390/organoids2040015/s1>, Figure S1: PCR genotyping of 35-day old HCOs; Figure S2: Quantitative RT-PCR analysis of 35-day old HCOs.; Table S1: DE-seq2 of 35d WT and SMAD1KO HCOs; Table S2: UP in WT co-expression analysis; Table S3: UP in SMAD1 KO co-expression analysis; Table S4: Oligos used in the study; Table S5: Antibodies used in the study.

Author Contributions: N.Q., A.D. and J.O.M. conceived the studies and wrote the manuscript. N.Q., A.D., B.J. and J.O.M. performed the experiments and analyses. All authors have read and agreed to the published version of the manuscript.

Funding: J.O.M. was funded by 1R56DK129575, 5U54CA210962-02, P30 DK123704, and P20GM130457.

Institutional Review Board Statement: Not applicable.

Informed Consent Statement: Not applicable.

Data Availability Statement: Primary RNA-sequencing files will be deposited to GEO.

Acknowledgments: We acknowledge support from the Medical University of South Carolina (MUSC) COBRE in Digestive & Liver Disease (CDLD) Cell Models Core. In addition, we acknowledge support from the MUSC Cell & Molecular Imaging Shared Resource.

Conflicts of Interest: The authors declare no conflict of interest.

References

1. Trisno, S.L.; Philo, K.E.D.; McCracken, K.W.; Cata, E.M.; Ruiz-Torres, S.; Rankin, S.A.; Han, L.; Nasr, T.; Chaturvedi, P.; Rothenberg, M.E.; et al. Esophageal Organoids from Human Pluripotent Stem Cells Delineate Sox2 Functions during Esophageal Specification. *Cell Stem Cell* **2018**, *23*, 501–515.e7. [[CrossRef](#)] [[PubMed](#)]
2. McCracken, K.W.; Aihara, E.; Martin, B.; Crawford, C.M.; Broda, T.; Treguier, J.; Zhang, X.; Shannon, J.M.; Montrose, M.H.; Wells, J.M. Wnt/beta-catenin promotes gastric fundus specification in mice and humans. *Nature* **2017**, *541*, 182–187. [[CrossRef](#)] [[PubMed](#)]
3. McCracken, K.W.; Cata, E.M.; Crawford, C.M.; Sinagoga, K.L.; Schumacher, M.; Rockich, B.E.; Tsai, Y.H.; Mayhew, C.N.; Spence, J.R.; Zavros, Y.; et al. Modelling human development and disease in pluripotent stem-cell-derived gastric organoids. *Nature* **2014**, *516*, 400–404. [[CrossRef](#)] [[PubMed](#)]
4. Spence, J.R.; Mayhew, C.N.; Rankin, S.A.; Kuhar, M.F.; Vallance, J.E.; Tolle, K.; Hoskins, E.E.; Kalinichenko, V.V.; Wells, S.I.; Zorn, A.M.; et al. Directed differentiation of human pluripotent stem cells into intestinal tissue in vitro. *Nature* **2011**, *470*, 105–109. [[CrossRef](#)]
5. Tsai, Y.H.; Nattiv, R.; Dedhia, P.H.; Nagy, M.S.; Chin, A.M.; Thomson, M.; Klein, O.D.; Spence, J.R. In vitro patterning of pluripotent stem cell-derived intestine recapitulates in vivo human development. *Development* **2017**, *144*, 1045–1055. [[CrossRef](#)]
6. Crespo, M.; Vilar, E.; Tsai, S.Y.; Chang, K.; Amin, S.; Srinivasan, T.; Zhang, T.; Pipalia, N.H.; Chen, H.J.; Witherspoon, M.; et al. Colonic organoids derived from human induced pluripotent stem cells for modeling colorectal cancer and drug testing. *Nat. Med.* **2017**, *23*, 878–884. [[CrossRef](#)]
7. Munera, J.O.; Sundaram, N.; Rankin, S.A.; Hill, D.; Watson, C.; Mahe, M.; Vallance, J.E.; Shroyer, N.F.; Sinagoga, K.L.; Zarzoso-Lacoste, A.; et al. Differentiation of Human Pluripotent Stem Cells into Colonic Organoids via Transient Activation of BMP Signaling. *Cell Stem Cell* **2017**, *21*, 51–64.e6. [[CrossRef](#)]
8. Zorn, A.M.; Wells, J.M. Vertebrate endoderm development and organ formation. *Annu. Rev. Cell Dev. Biol.* **2009**, *25*, 221–251. [[CrossRef](#)]
9. Sancho, E.; Batlle, E.; Clevers, H. Signaling pathways in intestinal development and cancer. *Annu. Rev. Cell Dev. Biol.* **2004**, *20*, 695–723. [[CrossRef](#)]
10. Shyer, A.E.; Huycke, T.R.; Lee, C.; Mahadevan, L.; Tabin, C.J. Bending gradients: How the intestinal stem cell gets its home. *Cell* **2015**, *161*, 569–580. [[CrossRef](#)]
11. Walton, K.D.; Whidden, M.; Kolterud, A.; Shoffner, S.K.; Czerwinski, M.J.; Kushwaha, J.; Parmar, N.; Chandrasekhar, D.; Freddo, A.M.; Schnell, S.; et al. Villification in the mouse: Bmp signals control intestinal villus patterning. *Development* **2016**, *143*, 427–436. [[CrossRef](#)] [[PubMed](#)]
12. Roberts, D.J.; Johnson, R.L.; Burke, A.C.; Nelson, C.E.; Morgan, B.A.; Tabin, C. Sonic Hedgehog Is an Endodermal Signal Inducing Bmp-4 and Hox Genes during Induction and Regionalization of the Chick Hindgut. *Development* **1995**, *121*, 3163–3174. [[CrossRef](#)] [[PubMed](#)]
13. Tiso, N.; Filippi, A.; Pauls, S.; Bortolussi, M.; Argenton, F. BMP signalling regulates anteroposterior endoderm patterning in zebrafish. *Mech. Dev.* **2002**, *118*, 29–37. [[CrossRef](#)] [[PubMed](#)]
14. Dye, B.R.; Hill, D.R.; Ferguson, M.A.; Tsai, Y.H.; Nagy, M.S.; Dyal, R.; Wells, J.M.; Mayhew, C.N.; Nattiv, R.; Klein, O.D.; et al. In vitro generation of human pluripotent stem cell derived lung organoids. *eLife* **2015**, *4*, e05098. [[CrossRef](#)]
15. Noto, F.K.; Determan, M.R.; Cai, J.; Cayo, M.A.; Mallanna, S.K.; Duncan, S.A. Aneuploidy is permissive for hepatocyte-like cell differentiation from human induced pluripotent stem cells. *BMC Res. Notes* **2014**, *7*, 437. [[CrossRef](#)]
16. Munera, J.O.; Wells, J.M. Generation of Gastrointestinal Organoids from Human Pluripotent Stem Cells. *Methods Mol. Biol.* **2017**, *1597*, 167–177. [[CrossRef](#)]
17. Watson, C.L.; Mahe, M.M.; Munera, J.; Howell, J.C.; Sundaram, N.; Poling, H.M.; Schweitzer, J.I.; Vallance, J.E.; Mayhew, C.N.; Sun, Y.; et al. An in vivo model of human small intestine using pluripotent stem cells. *Nat. Med.* **2014**, *20*, 1310–1314. [[CrossRef](#)]

18. Qu, N.; Jeffcoat, B.; Maity, P.; Christensen, R.K.; Munera, J.O. Retinoic Acid Promotes the In Vitro Growth, Patterning and Improves the Cellular Composition of Human Pluripotent Stem-Cell-Derived Intestinal Organoids. *Int. J. Mol. Sci.* **2022**, *23*, 8624. [[CrossRef](#)]
19. Ran, F.A.; Hsu, P.D.; Wright, J.; Agarwala, V.; Scott, D.A.; Zhang, F. Genome engineering using the CRISPR-Cas9 system. *Nat. Protoc.* **2013**, *8*, 2281–2308. [[CrossRef](#)]
20. Gunne-Braden, A.; Sullivan, A.; Gharibi, B.; Sheriff, R.S.M.; Maity, A.; Wang, Y.F.; Edwards, A.; Jiang, M.; Howell, M.; Goldstone, R.; et al. GATA3 Mediates a Fast, Irreversible Commitment to BMP4-Driven Differentiation in Human Embryonic Stem Cells. *Cell Stem Cell* **2020**, *26*, 693–706.e9. [[CrossRef](#)]
21. Wills, A.; Dickinson, K.; Khokha, M.; Baker, J.C. Bmp signaling is necessary and sufficient for ventrolateral endoderm specification in *Xenopus*. *Dev. Dyn. Off. Publ. Am. Assoc. Anat.* **2008**, *237*, 2177–2186. [[CrossRef](#)] [[PubMed](#)]
22. Sherwood, R.I.; Maehr, R.; Mazzone, E.O.; Melton, D.A. Wnt signaling specifies and patterns intestinal endoderm. *Mech. Dev.* **2011**, *128*, 387–400. [[CrossRef](#)] [[PubMed](#)]
23. Kumar, M.; Jordan, N.; Melton, D.; Grapin-Botton, A. Signals from lateral plate mesoderm instruct endoderm toward a pancreatic fate. *Dev. Biol.* **2003**, *259*, 109–122. [[CrossRef](#)]
24. Fei, T.; Xia, K.; Li, Z.; Zhou, B.; Zhu, S.; Chen, H.; Zhang, J.; Chen, Z.; Xiao, H.; Han, J.D.; et al. Genome-wide mapping of SMAD target genes reveals the role of BMP signaling in embryonic stem cell fate determination. *Genome Res.* **2010**, *20*, 36–44. [[CrossRef](#)]
25. Stevens, M.L.; Chaturvedi, P.; Rankin, S.A.; Macdonald, M.; Jagannathan, S.; Yukawa, M.; Barski, A.; Zorn, A.M. Genomic integration of Wnt/beta-catenin and BMP/Smad1 signaling coordinates foregut and hindgut transcriptional programs. *Development* **2017**, *144*, 1283–1295. [[CrossRef](#)] [[PubMed](#)]
26. Arnold, S.J.; Maretto, S.; Islam, A.; Bikoff, E.K.; Robertson, E.J. Dose-dependent Smad1, Smad5 and Smad8 signaling in the early mouse embryo. *Dev. Biol.* **2006**, *296*, 104–118. [[CrossRef](#)]
27. Tremblay, K.D.; Dunn, N.R.; Robertson, E.J. Mouse embryos lacking Smad1 signals display defects in extra-embryonic tissues and germ cell formation. *Development* **2001**, *128*, 3609–3621. [[CrossRef](#)]
28. Yang, X.; Castilla, L.H.; Xu, X.; Li, C.; Gotay, J.; Weinstein, M.; Liu, P.P.; Deng, C.X. Angiogenesis defects and mesenchymal apoptosis in mice lacking SMAD5. *Development* **1999**, *126*, 1571–1580. [[CrossRef](#)]
29. Chang, H.; Huylebroeck, D.; Verschuere, K.; Guo, Q.; Matzuk, M.M.; Zwijsen, A. Smad5 knockout mice die at mid-gestation due to multiple embryonic and extraembryonic defects. *Development* **1999**, *126*, 1631–1642. [[CrossRef](#)]
30. Wei, C.Y.; Wang, H.P.; Zhu, Z.Y.; Sun, Y.H. Transcriptional factors smad1 and smad9 act redundantly to mediate zebrafish ventral specification downstream of smad5. *J. Biol. Chem.* **2014**, *289*, 6604–6618. [[CrossRef](#)]
31. Orvis, G.D.; Jamin, S.P.; Kwan, K.M.; Mishina, Y.; Kaartinen, V.M.; Huang, S.; Roberts, A.B.; Umans, L.; Huylebroeck, D.; Zwijsen, A.; et al. Functional redundancy of TGF-beta family type I receptors and receptor-Smads in mediating anti-Mullerian hormone-induced Mullerian duct regression in the mouse. *Biol. Reprod.* **2008**, *78*, 994–1001. [[CrossRef](#)] [[PubMed](#)]
32. Lacroix, B.; Keding, M.; Simon-Assmann, P.; Rousset, M.; Zweibaum, A.; Haffen, K. Developmental pattern of brush border enzymes in the human fetal colon. Correlation with some morphogenetic events. *Early Hum. Dev.* **1984**, *9*, 95–103. [[CrossRef](#)] [[PubMed](#)]
33. Raul, F.; Lacroix, B.; Aprahamian, M. Longitudinal distribution of brush border hydrolases and morphological maturation in the intestine of the preterm infant. *Early Hum. Dev.* **1986**, *13*, 225–234. [[CrossRef](#)] [[PubMed](#)]

Disclaimer/Publisher’s Note: The statements, opinions and data contained in all publications are solely those of the individual author(s) and contributor(s) and not of MDPI and/or the editor(s). MDPI and/or the editor(s) disclaim responsibility for any injury to people or property resulting from any ideas, methods, instructions or products referred to in the content.